European Journal of Mechanics / A Solids 113 (2025) 105673

Contents lists available at ScienceDirect

European Journal of Mechanics / A Solids

journal homepage: www.elsevier.com/locate/ejmsol

Full length article

Optimal grading of elastic modulus at contact corners with friction with application in fibrillar adhesives

Shi-Wen Chen [a], Gang-Feng Wang [a], Michele Ciavarella [b,c,*]

[a] Xi'an Jiaotong University. Department of Engineering Mechanics, SVL and MMML, 710049 Xi'an, PR China
[b] Politecnico di BARI, DMMM department, Viale Gentile 182, 70126 Bari, Italy
[c] Hamburg University of Technology, Department of Mechanical Engineering, Am Schwarzenberg-Campus 1, 21073 Hamburg, Germany

ARTICLE INFO

Keywords:
Bio-inspired adhesion
Wedges
Graded materials
Friction
Contact

ABSTRACT

Recent studies have reported that micropillars composed of graded materials exhibit high adhesion performance in fibrillar adhesive systems. To uncover the origin of this enhanced performance and further promote the application of graded materials, we investigate the general contact mechanics of wedges composed of power-law graded materials. Our findings show that the stress singularity at the apex of the wedge can be eliminated by increasing the exponent of the power-law modulus. For cases with perfectly bonded interfaces, frictionless interfaces, and interfaces with Coulomb friction, the critical conditions for eliminating stress singularities are presented, thereby suggesting how to obtain optimal designs.

1. Introduction

In nature, many insects and lizards obtain the ability to climb on various kinds of surfaces by evolving fibrillar foot pad organs (Heepe et al., 2017; Autumn et al., 2000; Arzt et al., 2003; Ciavarella et al., 2019). These fibrillar foot pads always show strong adhesion performance and are mostly switchable. Understanding the origin of their superior adhesion performance and switchability can offer guidance to the design and optimization of bio-inspired artificial adhesive systems in, for example, wall-climbing robots (Kim et al., 2008; Henrey et al., 2014; Li et al., 2023) and perching-and-takeoff robots (Liu et al., 2023).

In the case of fibrillar surfaces made of soft elastomeric pillars, friction is inevitably quite strong (for smooth contact, shear stress can reach easily values near the elastic modulus) (Chateauminois and Fretigny, 2008). However, while for frictionless homogeneous flat-ended cylindrical fibril there is uniform pressure, for the more realistic assumption of fully sticking to a rigid substrate, the stress is singular at the edge of contact area (Khaderi et al., 2015), very close to the classical crack singularity. Due to the stress singularity, the behaviour is not remote from that of a crack of size equal to the contact radius and therefore there is a condition similar to brittle failure in Griffith cracks. One strategy to avoid the influence of edge singularity is adopting mushroom-shaped fibrils. Such geometry of fibrils is widely spread in Nature (Gorb and Varenberg, 2007). del Campo et al. were among the first to fabricate polydimethylsiloxane (PDMS) surfaces patterned with mushroom-shaped fibrils, and observed 20 times stronger adhesion than surfaces patterned with flat-ended cylindrical fibrils (del Campo et al., 2007). To explain the superior adhesion performance of mushroom-shaped fibrils, Spuskanyuk et al. carried out finite element simulations and found that in both frictionless or sticking case, the mushroom fibrils are less sensitive to edge defects due to the compliant flange (Spuskanyuk et al., 2008) and it is likely that mushrooms with optimally sized flanges fail rather by central defects (Sameoto et al., 2012).

Another route of optimizing the attachments is by a gradient of mechanical properties (Scholz et al., 2008; Peisker et al., 2013; Liu et al., 2017), which also permits decreasing the stress concentration at the corner. For example, inserting a soft tip (Yoon et al., 2011; Bahjepalli et al., 2017; Fischer et al., 2017; Gorumlu and Aksak, 2017) or a soft shell (Minsky and Turner, 2015; Tian et al., 2022) to fibrils, good adhesion performance can be achieved by utilizing composite structures. Recently, Zhu et al. fabricated fibrils composed of a specific class of Functional Graded Material (FGM) whose elastic modulus is gradually decreased from the centre to the perimeter of the fibril along the radial direction (Zhu et al., 2024). Their numerical and experimental results confirmed not only the high adhesion performance of their FGM, but also the stability of the high performance.

As the modulus at the corner can never be exactly zero, singularities at the very contact edge remain, but the magnitude of stress is much reduced by the effect of grading (Kossa et al., 2023). Indeed, the graded materials fabricated in the experiments of Zhu et al. exhibit the same degree of singularity as homogeneous materials near the contact

* Corresponding author at: Politecnico di BARI, DMMM department, Viale Gentile 182, 70126 Bari, Italy.
E-mail address: Mciava@poliba.it (M. Ciavarella).

https://doi.org/10.1016/j.euromechsol.2025.105673
Received 14 January 2025; Received in revised form 5 April 2025; Accepted 8 April 2025
Available online 23 April 2025
0997-7538/© 2025 The Authors. Published by Elsevier Masson SAS. This is an open access article under the CC BY license (http://creativecommons.org/licenses/by/4.0/).

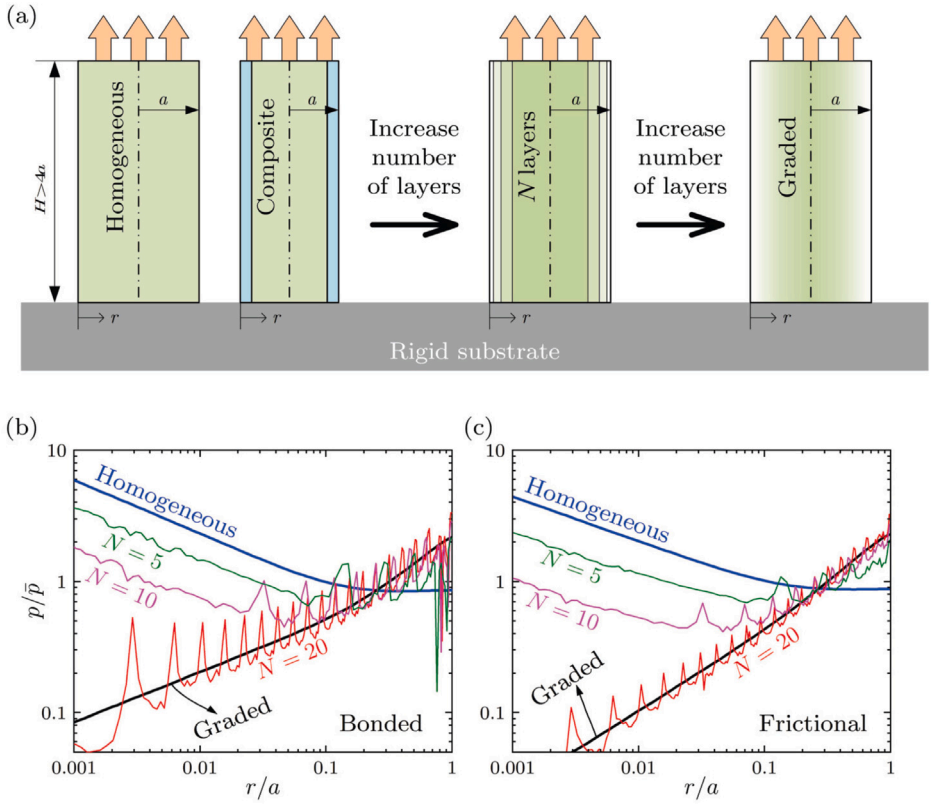

Fig. 1. (a) Schematic representation of the strategy for the approximate realization of power-law graded elastic modulus of fibrils. Pressure distribution for (b) perfectly bonded interfaces and (c) interfaces with Coulomb friction, where the coefficient of friction is 0.4.

edge (Fedorov and Matveenko, 2018), but a reduced stress intensity. However, as we tend towards the ideal condition of graded material with zero modulus at the corner, the stress singularity is completely eliminated, and both stress intensity and stress concentration in the classical sense disappear.

Hence, an approximate realization of the ideal graded material can be realized through composite layers (dos Reis et al., 2020), as schematically illustrated in Fig. 1(a). We add softer and softer layers on the outer side of the homogeneous fibrils, with the thickness of the outermost layer being k_1 ($k_1 < 1$) times that of the adjacent inner layer. Similarly, the elastic modulus of the outer layer is k_2 ($k_2 < 1$) times that of the adjacent inner layer. For example, take $k_1 = k_2 = 0.8$, then by increasing the number of layers N, the modulus at the central points of each layers approaches $E \propto r$, where r is the distance to the contact edge. Fig. 1(b) and (c) show the log–log plots between the contact pressure p, obtained by finite element simulations similar to Kossa et al. (2023), versus the distance r to the contact edge, for the cases when the fibrils are perfectly bonded to the rigid substrate or allowed to slip and controlled by Coulomb friction, respectively. Notice that pressure could be compressive during loading and negative upon unloading, where adhesion strength would be defined. The pressure is normalized by the mean pressure $\bar{p}$, and the distance to the contact edge is normalized by the contact radius a. In both bonded and frictional case, as discussed above, the singularity at the contact edge still exists for the composite fibrils, but the magnitude is reduced. Increasing N will further decrease the magnitude of stress, therefore the adhesion performance should increase as well. When N is increased to 20, it can be observed that the pressure distribution approaches very closely the pressure distribution curve of the continuous fibril with graded elastic modulus $E \propto r$, plotted as black solid lines. The composite fibril with 20 layers should have close adhesion performance to the continuous graded fibril, and can serve as an approximate realization of the graded material with linear elastic modulus.

Notice that the case discussed in Fig. 1 with linear grading of the modulus may not be optimal since the minimum power exponent for stress is positive which is reflected in a growing stress near the corner and a high stress concentration in the centre. One would be tempted to say that optimal is in general the case where singularity is just about cancelled but grading is not pushed further. This indeed may be the case if strength of the material locally does not depend on modulus. More discussion about this will be given later in the Discussion paragraph.

The discussion above suggests that fibrils with an appropriate power-law elastic modulus can be designed to exhibit high adhesion performance by eliminating the singularity at the contact edge, and such power-law graded materials can potentially be realized through multi-layer composite structures. By focusing on the region in the immediate vicinity of the contact edge and not restricting the angle to 90°, the problem can be generalized into a more general contact problem of wedges with arbitrary internal angle.

2. Solution for the stress distribution in the contact of wedges of graded material

Fig. 2 shows a semi-infinite wedge with an internal angle γ contacting with a rigid half-space, which is the situation representative of soft elastomeric (hence, incompressible) adhesive in contact with hard surfaces. The other surface of the wedge is free of traction. It is assumed that the wedge is made of elastic graded material with modulus varying in the radial direction as

$$E(r,\theta) = E_0 \left(\frac{r}{r_0}\right)^{\beta} \tag{1}$$

where r_0 is a characteristic length and E_0 denotes the elastic modulus at $r = r_0$.

Following the classical homogeneous wedge problem (Barber, 2002), and previous work of a graded elastic notch (Ciavarella, 2024), the

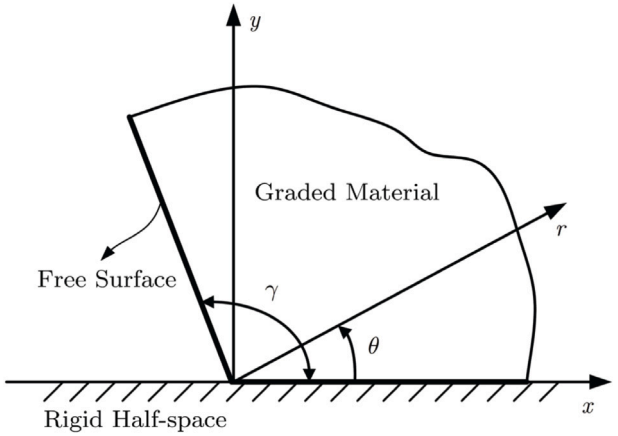

Fig. 2. Schematic representation of the contact between a rigid half-space a wedge composed of graded material.

boundary value problem can be solved by adopting an Airy stress function in the form of separated variables as

$$\varphi(r,\theta) = r^{\alpha+2} g(\theta) \tag{2}$$

Then the stress components vary as $\sigma \sim r^{\alpha}$ and can be expressed in polar coordinates as

$$\begin{aligned}\sigma_{rr}(r,\theta) &= \frac{1}{r}\frac{\partial \varphi(r,\theta)}{\partial r} + \frac{1}{r^2}\frac{\partial^2 \varphi(r,\theta)}{\partial \theta^2} \\ &= r^{\alpha}\left[(\alpha+2)\, g(\theta) + g''(\theta)\right]\end{aligned} \tag{3}$$

$$\sigma_{\theta\theta}(r,\theta) = \frac{\partial^2 \varphi(r,\theta)}{\partial r^2} = (\alpha+1)(\alpha+2) r^{\alpha} g(\theta) \tag{4}$$

$$\sigma_{r\theta}(r,\theta) = -\frac{\partial}{\partial r}\left(\frac{1}{r}\frac{\partial \varphi(r,\theta)}{\partial \theta}\right) = -(\alpha+1) r^{\alpha} g'(\theta) \tag{5}$$

Under plane strain conditions, the constitutive equations are

$$\varepsilon_{rr} = \frac{1-\nu^2}{E(r,\theta)}\left(\sigma_{rr} - \frac{\nu}{1-\nu}\sigma_{\theta\theta}\right) \tag{6}$$

$$\varepsilon_{\theta\theta} = \frac{1-\nu^2}{E(r,\theta)}\left(\sigma_{\theta\theta} - \frac{\nu}{1-\nu}\sigma_{rr}\right) \tag{7}$$

$$\varepsilon_{r\theta} = \frac{1+\nu}{E(r,\theta)}\sigma_{r\theta} \tag{8}$$

where ν is the Poisson's ratio and is assumed to be constant. For soft materials, Poisson's ratio is given as $\nu = 0.5$. The strains need to satisfy the compatibility equation as

$$\frac{\partial^2 \varepsilon_{\theta\theta}}{\partial r^2} + \frac{1}{r^2}\frac{\partial^2 \varepsilon_{rr}}{\partial \theta^2} + \frac{2}{r}\frac{\partial \varepsilon_{\theta\theta}}{\partial r} - \frac{1}{r}\frac{\partial \varepsilon_{rr}}{\partial r} = \frac{2}{r}\frac{\partial^2 \varepsilon_{r\theta}}{\partial r \partial \theta} + \frac{2}{r^2}\frac{\partial \varepsilon_{r\theta}}{\partial \theta} \tag{9}$$

and this leads to a fourth order ordinary differential equation (ODE) for $g(\theta)$

$$\begin{aligned}&(2+\alpha)(\alpha-\beta)\left[\beta+\alpha(-2-\alpha+\beta)+(2+\alpha)(\alpha-\beta)\nu\right] g(\theta) \\ &+\left[-4+\beta-2\alpha^2(1-\nu)-2\alpha(2-\beta)(1-\nu)+\left(4+\beta^2\right)\nu\right] g''(\theta) \\ &-(1-\nu) g^{IV}(\theta) = 0\end{aligned} \tag{10}$$

The general solution of the ODE can be written as a combination of four linearly independent particular solutions as

$$g(\theta) = C_1 g_1(\theta) + C_2 g_2(\theta) + C_3 g_3(\theta) + C_4 g_4(\theta) \tag{11}$$

with the specific form determined by the nature of characteristic roots, see appendix A for details. Then, the factors C_i can be determined by boundary conditions. Two different conditions of the interface between the wedge and the rigid half-space are considered: a perfectly bonded interface and an interface with Coulomb friction.

2.1. The solution for a perfectly bonded interface

The boundary conditions at the free surface $\theta = \gamma$ are

$$\sigma_{\theta\theta}(\gamma) = (\alpha+1)(\alpha+2) r^{\alpha} g(\gamma) = 0 \tag{12}$$

$$\sigma_{r\theta}(\gamma) = -(\alpha+1) r^{\alpha} g'(\gamma) = 0 \tag{13}$$

At the bonded interface where $\theta = 0$, the displacement continuity conditions require that $u_{\theta}(r,0) = u_r(r,0) = 0$. Knowing that the geometric equations in polar coordinates are

$$\varepsilon_{rr} = \frac{\partial u_r}{\partial r} \tag{14}$$

$$\varepsilon_{\theta\theta} = \frac{1}{r}\frac{\partial u_{\theta}}{\partial \theta} + \frac{u_r}{r} \tag{15}$$

$$2\varepsilon_{r\theta} = \frac{1}{r}\frac{\partial u_r}{\partial \theta} + \frac{\partial u_{\theta}}{\partial r} - \frac{u_{\theta}}{r} \tag{16}$$

then the boundary conditions when $\theta = 0$ can be written as

$$\frac{\partial^2 u_{\theta}}{\partial r^2} = 2\frac{\partial \varepsilon_{r\theta}}{\partial r} + \frac{2}{r}\varepsilon_{r\theta} - \frac{1}{r}\frac{\partial \varepsilon_{rr}}{\partial \theta} = 0 \tag{17}$$

$$\frac{\partial u_r}{\partial r} = \varepsilon_{rr} = 0 \tag{18}$$

Transforming from the displacement conditions to the conditions of their partial derivatives, Eq. (17) and (18), will only introduce rigid body displacement and rotation, which do not affect the stress solution (Barber, 2002).

The boundary conditions Eq. (12), (13), (17) and (18) consist in a system of four linear equations on the factors C_i, and the equations having non-zero solutions requires that the determinant of the coefficient matrix is zero. From this, we can determine the possible values of α.

2.2. The solution for an interface with Coulomb friction

At the free surface, the boundary conditions remain the same as those described in Eq. (12) and (13). At the interface, sliding occurs under Coulomb friction. The boundary condition $u_{\theta}(r,0) = 0$, which is related to Eq. (17), still applies. The traction condition is given by

$$\sigma_{r\theta} = \mu \sigma_{\theta\theta} \tag{19}$$

where μ is the friction coefficient, and its sign depends on the direction of sliding. Similar to the case of a bonded interface, Eq. (12), (13), (17) and (19) form a system of equations for the factors C_i, where α is determined by setting the determinant to zero.

3. Results

Before presenting the results, validation of our method must be performed. When the exponent β in the modulus is set to 0, the contact problem investigated in this study reduces to the classical homogeneous problem. This problem has been extensively studied by Gdoutos and Theocaris (Gdoutos and Theocaris, 1975) as well as Churchman et al. Churchman et al. (2003). Our derivation for $\beta = 0$ yields results that are identical to those reported in their works for various internal angles of the wedge, for both bonded interfaces and frictional interface with different coefficient of friction.

Moreover, we perform direct simulations of the contact of graded wedges to verify our analytical results, utilizing the finite element method (FEM) implemented in the commercial software Abaqus. Two specific cases are simulated. In the first case, the wedge is modelled as a sector with an internal angle of $\gamma = 90°$, with one surface perfectly bonded and the other traction-free. A uniform σ_{rr} is applied as the boundary condition at the distant circular arc, with the radius of the sector chosen as the characteristic length r_0 of the graded modulus. The sector is discretized into 18179 four-node plane strain elements

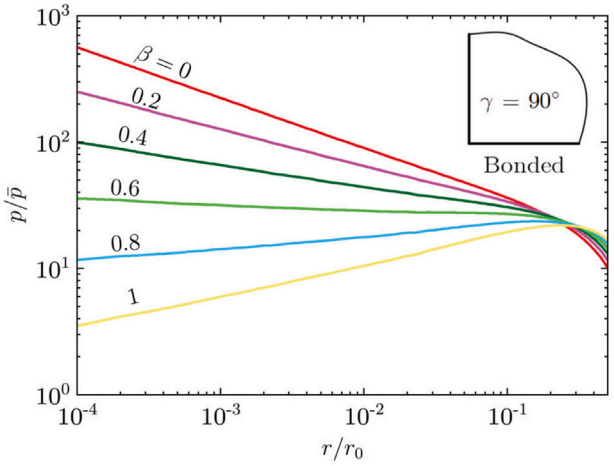

Fig. 3. The log–log plots of the pressure obtained from FEM simulations for $\gamma = 90°$ with a bonded interface.

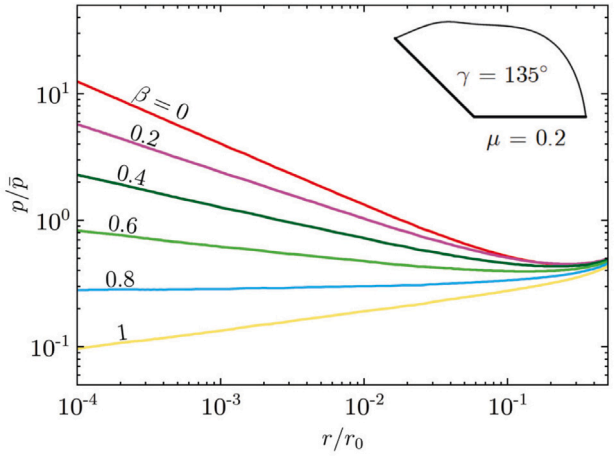

Fig. 4. The log–log plots of the pressure obtained from FEM simulations for $\gamma = 90°$ and $\mu = 0.2$.

(CPE4) with 18464 nodes, and the mesh near the apex is refined by several orders of magnitude. The second case involves a sector with an internal angle of $\gamma = 135°$, discretized into 26989 CPE4 elements containing 27281 nodes. In this case, the distant circular arc is fixed, while an analytical rigid plane is pressed against one surface and moved laterally with a friction coefficient of $\mu = 0.2$. In both cases, the power-law modulus described by Eq. (1) is implemented through a user material (UMAT) subroutine, and simulations are conducted for $\beta = 0, 0.2, 0.4, 0.6, 0.8, 1$.

Figs. 3 and 4 present the log–log plots of the pressure at the interface obtained from FEM simulations for the cases of $\gamma = 90°$ with a bonded interface and $\gamma = 135°$ with a frictional interface ($\mu = 0.2$), respectively. In the close vicinity of the apex, it can be observed that $\log p$ and $\log r$ exhibit a linear relation, indicating that the stresses should follow $\sigma \sim r^{\alpha}$ as assumed. By fitting the slope of the $\log p$ - $\log r$ relationship, the value of α can be determined. The results show that increasing the value of β in the modulus can transform α from negative to positive values, thereby eliminating the stress singularity. In Fig. 5, the values of α obtained from our analytical analyses are plotted alongside the FEM results as a function of β, and the analytical results closely align with the FEM results.

The stress components should in fact be a superposition of a series of Eq. (3), Eq. (4) or Eq. (5), respectively, with possible values of α determined as described earlier. Nonetheless, in the close vicinity of

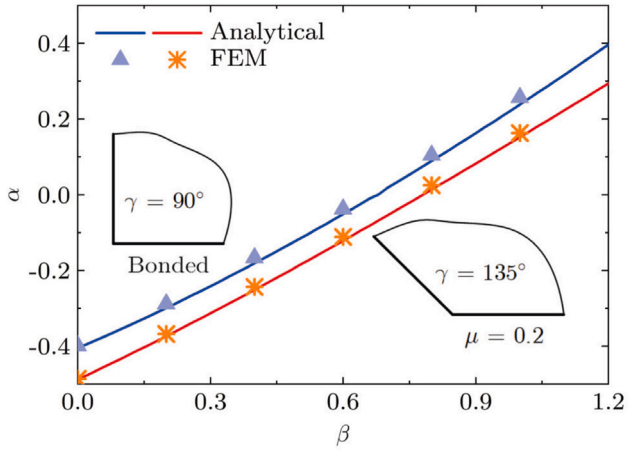

Fig. 5. The values of α as a function of β obtained for analytical analyses and FEM simulations.

the wedge apex, where r is sufficiently small, the variation of stress components with r is primarily governed by the term associated with the smallest solution of α. To ensure that the strain energy remains finite within a finite volume, α must satisfy the condition $\alpha > -1 + \beta/2$ (Ciavarella, 2024). Furthermore, it can be proved that $\alpha = 0$ is always a solution by substituting Eq. (A.9) into the boundary conditions. It is worth noting that even when $\alpha = 0$ is the smallest solution, the presence of the term $\sigma \sim r^0$ (*i.e.*, independent of r) depends on the far boundary conditions. This is evident in Figs. 3 and 4, where the pressure near the edge drops to 0 instead of remaining non-zero for $\beta = 0.8$ and 1. In these cases, while $\alpha = 0$ is the smallest solution, it does not manifest itself. In contrast, for a homogeneous flat-ended pillar in frictionless contact with a rigid plane ($\beta = 0, \gamma = 90°, \mu = 0$), the pressure is uniform (Spuskanyuk et al., 2008), and the term $\sigma \sim r^0$ dominates. Below, the solution $\alpha = 0$ will not be shown for simplicity.

Fig. 6 presents the contour map of solutions of α for different internal angle γ of the wedge and the exponent β of the graded material under perfectly bonded interface conditions. For a given angle γ, it is observed that $\alpha < 0$ for homogeneous case ($\beta = 0$), indicating a stress singularity near the apex of wedge. As β increases gradually, the singularity diminishes until α reaches 0, where the singularity is completely eliminated. The contour line where $\alpha = 0$ is highlighted with a bold line, representing the critical threshold for eliminating the singularity.

Fig. 7 illustrates the contour map of the solutions of α for the frictionless interface case, where the coefficient of friction μ is set to 0. Unlike the perfectly bonded case, no singularity is observed when the angle $\gamma \leq 90°$. When $\gamma = 180°$, the wedge problem corresponds to a mode I crack, and the singularity at the crack tip can also be eliminated by using graded material. When γ is small, it can be observed that $\alpha = \beta$ will always be the solution.

When a pillar is retracted from a rigid substrate, the contact area shrinks due to volume conservation. If slipping is allowed and the friction force is governed by Coulomb law, the stresses $\sigma_{r\theta}$ and $\sigma_{\theta\theta}$ at the interface will both be positive. In this case, the coefficient of friction μ is positive. Figs. 8 and 9 present the contour maps of α for $\mu = 0.2$ and $\mu = 0.5$ respectively. For homogeneous pillar, where $\gamma = 90°$ and $\beta = 0$, the stress is singular for both $\mu = 0.2$ and $\mu = 0.5$. This explains why homogeneous pillars are not optimal for fibrillar adhesion in frictional case, and also, using graded materials can eliminate the singularity and enhance adhesion performance. The contour line for $\alpha = 0$ in the case $\mu = 0.2$ is monotonic. Specifically, for larger angle γ, the exponent β of the graded material must be larger to eliminate singularity. However, in the case of $\mu = 0.5$, the boundary for $\alpha = 0$ is non-monotonic, which is similar to the perfectly bonded case. Compared to the case where

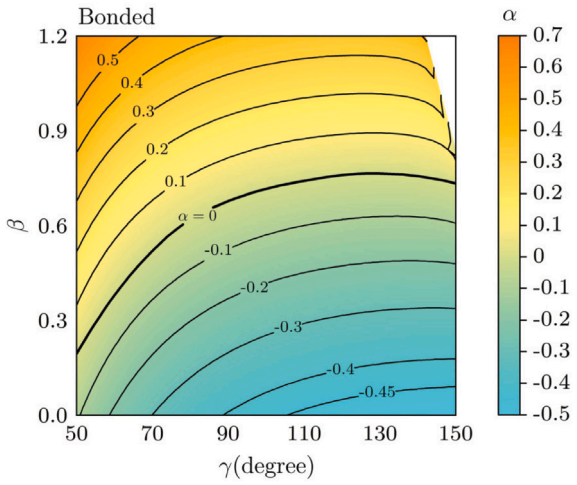

Fig. 6. Contour map of the solutions of α as a function of γ and β when the interface is perfectly bonded.

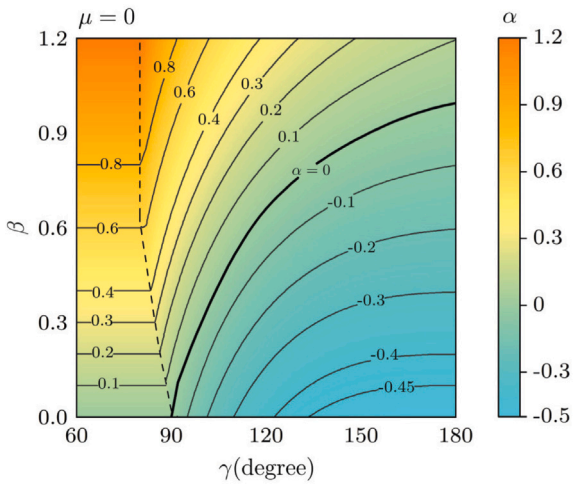

Fig. 7. Contour map of the solutions of α as a function of γ and β when $\mu = 0$.

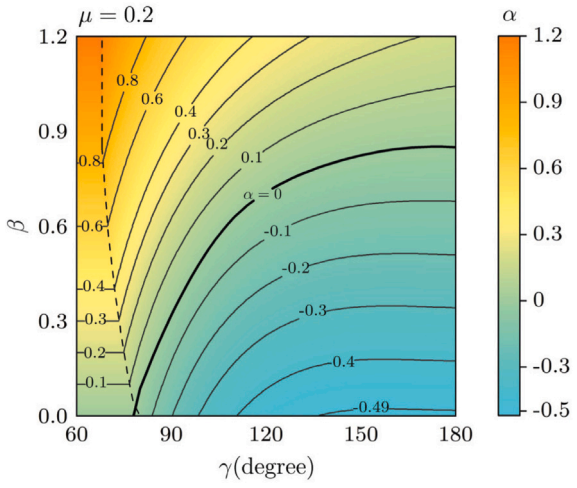

Fig. 8. Contour map of the solutions of α as a function of γ and β when $\mu = 0.2$.

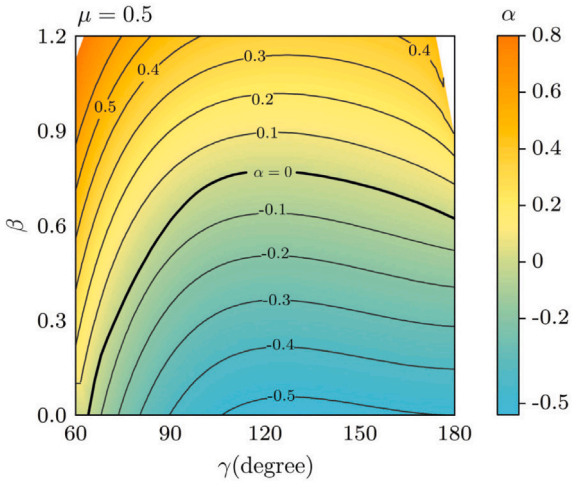

Fig. 9. Contour map of the solutions of α as a function of γ and β when $\mu = 0.5$.

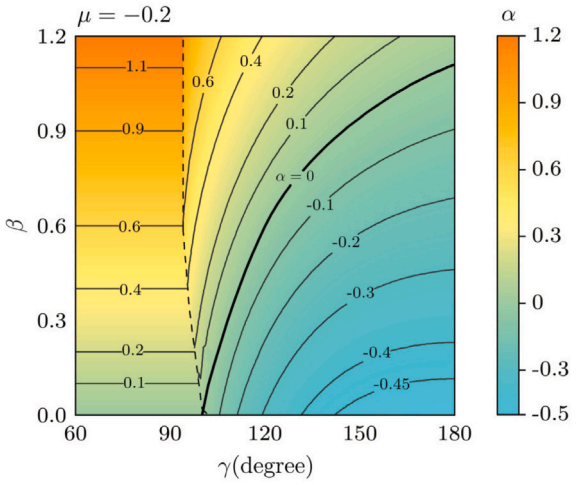

Fig. 10. Contour map of the solutions of α as a function of γ and β when $\mu = -0.2$.

$\mu = 0$, increasing μ will decrease the area where $\alpha = \beta$, and when μ is large enough, the contour map will be similar to the bonded case.

It is also possible for the coefficient of friction μ be negative. If the wedge is pressed against the rigid plane and moved laterally along the positive x-direction, it can be observed that at the interface, $\sigma_{\theta\theta}$ is negative while $\sigma_{r\theta}$ is positive, resulting in a negative μ. Figs. 10 and 11 present the contour maps of α for $\mu = -0.2$ and $\mu = -0.5$, respectively. In the case of the pillar where $\gamma = 90°$, no singularity appears at the apex of the wedge when the material is homogeneous ($\beta = 0$). This leads to an interesting phenomenon: when a pillar is pressed against a rigid plane and slides, the leading edge (*i.e.* the edge in front of the sliding direction) exhibits a positive μ with a singularity in stress, while the trailing edge (*i.e.* the edge behind the sliding direction) shows a negative μ with no singularity in stress. To eliminate the singularity, only the leading edge need to be addressed. However, for a trapezoidal fibril with an angle γ close to 180°, both the leading and trailing edges exhibit singularities, and a larger value of β is required to eliminate the singularity at the trailing edge.

From the calculations above, the values of β corresponding to turning α from negative to positive can be determined. These values, denoted as β_c, represent the critical values for eliminating the singularity at the apex. Fig. 12 presents a 3-D plot of β_c as a function of

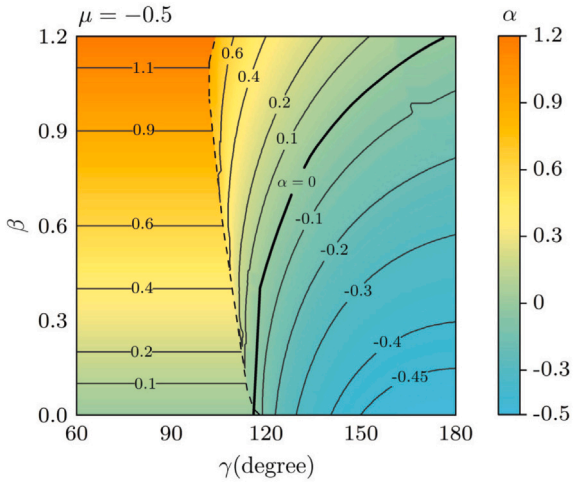

Fig. 11. Contour map of the solutions of α as a function of γ and β when $\mu = -0.5$.

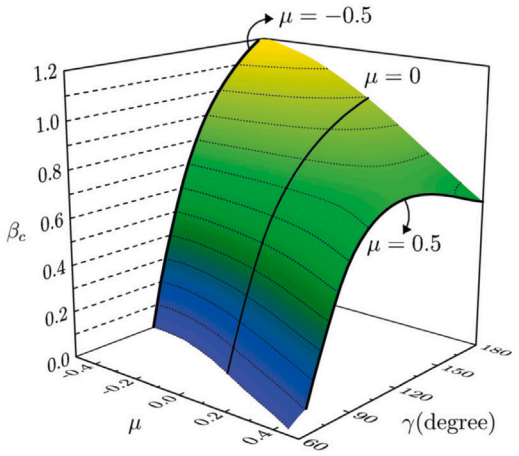

Fig. 12. Critical value of β for singularity elimination as a function of μ and γ.

the coefficient of friction μ and the internal angle γ. Contour lines are plotted for $\beta_c = 0$ and increasing in steps of 0.1. This figure ultimately provides a comprehensive critical condition for eliminating singularity, where $\beta > \beta_c$ is required.

Looking back to the mushroom-shaped fibril, we find that another source of its superior adhesion performance is its insensitivity to crack propagation. For the homogeneous pillar, the energy release rate will increase as the edge crack propagates, leading to further acceleration of crack growth, while utilizing mushroom-shaped geometry can prevent this (Spuskanyuk et al., 2008). Qualitatively speaking, utilizing graded material that introduces a significantly softer area at the edge results in a smoother variation of the energy release rate, leading to a reduction in crack sensitivity. This warrants further quantitative research in the future.

4. Discussion

As in two previous papers about elimination of stress singularity in a notch (Ciavarella, 2024, 2025) the problem of optimizing the grading of the elastic modulus is non trivial. Indeed let us return to the case of discrete number of layers of Fig. 1 where we assume the standard singular stress remains which is

$$\frac{p}{\bar{p}} = C\left(\frac{r}{a}\right)^{-0.406} \tag{20}$$

where the stress intensity C is reduced with respect to the homogeneous case. In this case as done by Kossa et al. we can assume that the surface energy w is independent on the local modulus (considering it to be a property of the interface) and define the improvement by comparing the strength of the singularity in the graded punch C_{grad} with that of the homogeneous punch with modulus equal to the outermost modulus of the graded punch C_{hom}. Since C_{hom} does not depend on elastic modulus, but only on geometry (in particular here only the ratio of the height of the pillar H over the pillar radius a), this criterion used by Kossa et al. corresponds to observing the stress concentration as in Fig. 1. It is clear that if the number of layers becomes large, this condition looses sense, since the stress concentration may become very low at the edge, and larger away from it.

In the case of a true power law graded modulus, the criteria discussed in the case of a graded notch (Ciavarella, 2024, 2025) apply. In particular, we may consider strength as power law of the modulus

$$p_{allow} = SE^s \tag{21}$$

where S, s are material constants. In this equation, s is called *strength-modulus exponent ratio:* we expect $s < 1$ to be more frequent, since in particular the limit case $s = 0$, corresponds to structural optimization as *identical* to stress concentration minimization — as in Kossa et al.

As we get singularity in stress α, namely that $p(r) = p_0 r^{\alpha(\beta)}$, we can apply a local condition of strength, as

$$p_{allow}(r) = SE^s = SE_0^s\left(\frac{r}{r_0}\right)^{\beta s} \tag{22}$$

and hence

$$p(r)/p_{allow}(r) = \frac{p_0 r^{\alpha(\beta)}}{SE_0^s\left(\frac{r}{r_0}\right)^{\beta s}} = C_1 r^{\alpha(\beta)-\beta s} \tag{23}$$

where C_1 is a constant. Hence, as in Ciavarella (2024, 2025) we can keep the condition of strength satisfied at all points (in the singular region) $p/p_{allow} < 1$ if

$$\alpha(\beta) > \beta s \tag{24}$$

and in particular optimal design corresponds to

$$\alpha_{optimal}(\beta) = \beta s \tag{25}$$

If $s = 0$, the criterion corresponds to stress minimization, and we just design as to cancel the singularity. If instead $s > 0$, we need to push the grading further and obtain an increasing stress from the corner, as indicated in (25).

5. Conclusions

In this work, we investigated the adhesive contact problem between a rigid half-space and a wedge composed of power-law graded elastic materials. Comprehensive theoretical analyses are conducted to determine the stress dependence on the distance to the apex of the wedge for varying internal angles γ and power-law exponents β. The degree of stress singularity is evaluated for both perfectly bonded interfaces and interfaces with Coulomb friction. FEM simulations are performed and the results align closely with the analytical findings. Critical lines for eliminating stress singularities are identified. In the bonded case and for cases with a large positive coefficient of friction ($\mu = 0.5$), the critical lines are non-monotonic, with the critical value of β required to eliminate singularities initially increasing with γ and then decreasing. For cases with negative μ or small positive μ ($\mu = 0, \mu = 0.2$), the critical lines are monotonic, with the critical value of β reaching its maximum at $\gamma = 180°$. As eliminating stress singularity is a key factor for the high adhesion performance of micropillars made from graded materials, the present comprehensive results should be a useful guide.

CRediT authorship contribution statement

Shi-Wen Chen: Writing – original draft, Visualization, Software, Investigation, Formal analysis, Data curation. **Gang-Feng Wang:** Writing – review & editing, Supervision, Investigation, Funding acquisition. **Michele Ciavarella:** Writing – review & editing, Validation, Supervision, Methodology, Conceptualization.

Declaration of competing interest

The authors declare that they have no known competing financial interests or personal relationships that could have appeared to influence the work reported in this paper.

Acknowledgements

M.C. was partly supported by the Italian Ministry of University and Research under the Programme "Department of Excellence" Legge 232/2016 (Grant No. CUP - D93C23000100001). G.F.W. and S.W.C. acknowledge support from the National Natural Science Foundation of China (Grant No. 12372100).

Appendix. The general solutions for the ODE (10)

Eq. (10) is a fourth order ODE, with its characteristic roots might be real or complex, distinct or repeated, depending on the value of α, β and ν. The nature of the characteristic roots will determine the form of the general solution.

In this paper, the graded material is assumed to be incompressible, so $\nu = 0.5$. In the following, we present the characteristic roots and the general solutions for $0 < \beta < -1 + \sqrt{5}$ and $\alpha > -1 + \beta/2$. We can find

$$\alpha_c = -1 + \frac{\beta}{2} + \frac{\beta}{\sqrt{2}}\sqrt{\frac{2-\beta^2}{4-\beta^2}} \tag{A.1}$$

Then, the following cases necessary for our analysis are considered:

(1) $-1 + \beta/2 < \alpha < \alpha_c$, then all four characteristic roots are complex numbers. We have

$$\begin{aligned} x_{1,2} &= b_1 \pm i a_1 \\ x_{3,4} &= -b_1 \pm i a_1 \end{aligned} \tag{A.2}$$

and

$$\begin{aligned} g(\theta) = &\exp(b_1\theta)\left[C_1\cos(a_1\theta) + C_2\sin(a_1\theta)\right] \\ &+ \exp(-b_1\theta)\left[C_3\cos(a_1\theta) + C_4\cos(a_1\theta)\right] \end{aligned} \tag{A.3}$$

(2) $\alpha = \alpha_c$, then we have two repeated imaginary roots as

$$\begin{aligned} x_{1,2} &= i a_1 \\ x_{3,4} &= -i a_1 \end{aligned} \tag{A.4}$$

Therefore the general solution is

$$g(\theta) = \left(C_1 + C_2\theta\right)\cos(a_1\theta) + \left(C_3 + C_4\theta\right)\sin(a_1\theta) \tag{A.5}$$

(3) $\alpha_c < \alpha < 0$ or $\alpha > \beta$, we have four imaginary roots as

$$\begin{aligned} x_{1,2} &= \pm i a_1 \\ x_{3,4} &= \pm i a_2 \end{aligned} \tag{A.6}$$

and the general solution is

$$g(\theta) = C_1\cos(a_1\theta) + C_2\sin(a_1\theta) + C_3\cos(a_2\theta) + C_4\sin(a_2\theta) \tag{A.7}$$

(4) $\alpha = 0$ or $\alpha = \beta$. The roots are

$$\begin{aligned} x_{1,2} &= 0 \\ x_{3,4} &= \pm i a_1 \end{aligned} \tag{A.8}$$

and the general solution is

$$g(\theta) = C_1 + C_2\theta + C_3\cos(a_1\theta) + C_4\sin(a_1\theta) \tag{A.9}$$

(5) $0 < \alpha < \beta$. The roots are

$$\begin{aligned} x_{1,2} &= \pm b_1 \\ x_{3,4} &= \pm i a_2 \end{aligned} \tag{A.10}$$

and the general solution is

$$g(\theta) = C_1\exp(b_1\theta) + C_2\exp(-b_1\theta) + C_3\cos(a_2\theta) + C_4\sin(a_2\theta) \tag{A.11}$$

Data availability

Data will be made available upon request.

References

Arzt, E., Gorb, S., Spolenak, R., 2003. From micro to nano contacts in biological attachment devices. Proc. Natl. Acad. Sci. USA 100 (19), 10603–10606.
Autumn, K., et al., 2000. Adhesive force of a single gecko foot-hair. Nature 405 (6787), 681–685.
Bahjepalli, R.G., et al., 2017. Numerical study of adhesion enhancement by composite fibrils with soft tip layers. J. Mech. Phys. Solids 99, 357–378.
Barber, J.R., 2002. Elasticity. Kluwer Academic Publishers.
del Campo, A., Greiner, C., Arzt, E., 2007. Contact shape controls adhesion of bioinspired fibrillar surfaces. Langmuir 23 (20), 10235–10243.
Chateauminois, A., Fretigny, C., 2008. Local friction at a sliding interface between an elastomer and a rigid spherical probe. Eur. Phys. J. E 27 (2), 221–227.
Churchman, C., Mugadu, A., Hills, D.A., 2003. Asymptotic results for slipping complete frictional contacts. Eur. J. Mech. A - Solids 22 (6), 793–800.
Ciavarella, M., 2024. Cancelling the effect of sharp notches or cracks with graded elastic modulus materials. J. Mech. Phys. Solids 192, 105809.
Ciavarella, M., 2025. A graded elastic modulus concept to eliminate stress or strain energy density singularity at sharp notches and cracks, with consequent elimination of size-scale effect on strength. Eur. J. Mech. A Solids 109, 105477.
Ciavarella, M., et al., 2019. The role of adhesion in contact mechanics. J. R. Soc. Interface 16 (151), 20180738.
Fedorov, A.Y., Matveenko, V.P., 2018. Investigation of stress behavior in the vicinity of singular points of elastic bodies made of functionally graded materials. J. Appl. Mechanics- Trans. the Asme 85 (6), 061008.
Fischer, S.C.L., Arzt, E., Hensel, R., 2017. Composite pillars with a tunable interface for adhesion to rough substrates. ACS Appl. Mater. & Interfaces 9 (1), 1036–1044.
Gdoutos, E.E., Theocaris, P.S., 1975. Stress-concentrations at apex of a plane indenter acting on an elastic half plane. J. Appl. Mechanics- Trans. the Asme 42 (3), 688–692.
Gorb, S.N., Varenberg, M., 2007. Mushroom-shaped geometry of contact elements in biological adhesive systems. J. Adhes. Sci. Technol. 21 (12–13), 1175–1183.
Gorumlu, S., Aksak, B., 2017. Sticking to rough surfaces using functionally graded bio-inspired microfibres. R. Soc. Open Sci. 4 (6), 161105.
Heepe, L., Xue, L., Gorb, S.N., 2017. Bio-Inspired Structured Adhesives. Springer Nature.
Henrey, M., et al., 2014. Abigaille-III: A versatile, bioinspired hexapod for scaling smooth vertical surfaces. J. Bionic Eng. 11 (1), 1–17.
Khaderi, S.N., et al., 2015. Detachment of an adhered micropillar from a dissimilar substrate. J. Mech. Phys. Solids 75, 159–183.
Kim, S., et al., 2008. Smooth vertical surface climbing with directional adhesion. IEEE Trans. Robot. 24 (1), 65–74.
Kossa, A., Hensel, R., McMeeking, R.M., 2023. Adhesion of a cylindrical punch with elastic properties that vary radially. Mech. Res. Commun. 130, 104123.
Li, Q., et al., 2023. An aerial-wall robotic insect that can land, climb, and take off from vertical surfaces. Research 6, 0144.
Liu, Z.Q., et al., 2017. Functional gradients and heterogeneities in biological materials: Design principles, functions, and bioinspired applications. Prog. Mater. Sci. 88, 467–498.
Liu, H.R., et al., 2023. Electrically active smart adhesive for a perching-and-takeoff robot. Sci. Adv. 9 (43), eadj3133.
Minsky, H.K., Turner, K.T., 2015. Achieving enhanced and tunable adhesion via composite posts. Appl. Phys. Lett. 106 (20), 201604.
Peisker, H., Michels, J., Gorb, S.N., 2013. Evidence for a material gradient in the adhesive tarsal setae of the ladybird beetle *Coccinella septempunctata*. Nat. Commun. 4, 1661.
dos Reis, M.Q., et al., 2020. Functionally graded adherends in adhesive joints: An overview. J. Adv. Join. Process. 2, 100033.
Sameoto, D., Sharif, H., Menon, C., 2012. Investigation of low-pressure adhesion performance of mushroom shaped biomimetic dry adhesives. J. Adhes. Sci. Technol. 26 (23), 2641–2652.

Scholz, I., Baumgartner, W., Federle, W., 2008. Micromechanics of smooth adhesive organs in stick insects: pads are mechanically anisotropic and softer towards the adhesive surface. J. Comp. Physiol. A- Neuroethol. Sens. Neural Behav. Physiol. 194 (4), 373–384.

Spuskanyuk, A.V., et al., 2008. The effect of shape on the adhesion of fibrillar surfaces. Acta Biomater. 4 (6), 1669–1676.

Tian, H.M., et al., 2022. Core–shell dry adhesives for rough surfaces via electrically responsive self-growing strategy. Nat. Commun. 13 (1), 7659.

Yoon, H., et al., 2011. Polymeric nanopillars reinforced with metallic shells in the Lower Stem Region. Small 7 (21), 3005–3010.

Zhu, B., et al., 2024. Micropillar with radial gradient modulus enables robust adhesion and friction. Small 20 (30), 2310887.